Research Article | Vol. 9, No. 12 | 1 Dec 2018 | BIOMEDICAL OPTICS EXPRESS 6400
Biomedical Optics EXPRESS

Integrated RFA/PSOCT catheter for real-time guidance of cardiac radio-frequency ablation

XIAOWEI ZHAO,[1,6] XIAOYONG FU,[1,6] COLIN BLUMENTHAL,[2] YVES T. WANG,[1,3] MICHAEL W. JENKINS,[1,3] CHRISTOPHER SNYDER,[3,4] MAURICIO ARRUDA,[5] AND ANDREW M. ROLLINS[1,*]

[1]*Department of Biomedical Engineering, Case Western Reserve University, Cleveland, OH 44106, USA*
[2]*School of Medicine, Case Western Reserve University, Cleveland, OH 44106, USA*
[3]*Department of Pediatrics, Case Western Reserve University, Cleveland, OH 44106, USA*
[4]*Rainbow Babies and Children's Hospital, Division of Pediatric Cardiology, University Hospitals, Cleveland, OH 44106, USA*
[5]*Department of Cardiology, University Hospitals Case Medical Center, Cleveland, OH 44120, USA*
[6]*authors contributed equally*
**rollins@case.edu*

Abstract: Radiofrequency ablation (RFA) is an important standard therapy for cardiac arrhythmias, but direct monitoring of tissue treatment is currently lacking. We demonstrate an RFA catheter integrated with polarization sensitive optical coherence tomography (PSOCT) for directly monitoring the RFA process in real time. The integrated RFA/OCT catheter was modified from a standard clinical RFA catheter and includes a miniature forward-viewing cone-scanning OCT probe. The PSOCT system was validated with a quarter-wave plate while the RFA function of the integrated catheter was validated by comparing lesion sizes with those made with an unmodified RFA catheter. Additionally, the integrated catheter guided catheter-tissue apposition and monitored RFA lesion formation in cardiac tissue in real time. The results show that catheter-tissue contact can be characterized by observing the features of the blood and tissue in the acquired OCT images and that RFA lesion formation can be confirmed by monitoring the change in phase retardance in the acquired PSOCT images. This system demonstrates the feasibility of an integrated RFA/OCT catheter to deliver RF energy and image the cardiac wall simultaneously and justifies further research into use of this technology to aid RFA therapy for cardiac arrhythmias.

OCIS codes: (110.4500) Optical coherence tomography; (170.2150) Endoscopic imaging; (170.3890) Medical optics instrumentation.

References and links

1. D. Mozaffarian, E. J. Benjamin, A. S. Go, D. K. Arnett, M. J. Blaha, M. Cushman, S. R. Das, S. de Ferranti, J. P. Després, H. J. Fullerton, V. J. Howard, M. D. Huffman, C. R. Isasi, M. C. Jiménez, S. E. Judd, B. M. Kissela, J. H. Lichtman, L. D. Lisabeth, S. Liu, R. H. Mackey, D. J. Magid, D. K. McGuire, E. R. Mohler 3rd, C. S. Moy, P. Muntner, M. E. Mussolino, K. Nasir, R. W. Neumar, G. Nichol, L. Palaniappan, D. K. Pandey, M. J. Reeves, C. J. Rodriguez, W. Rosamond, P. D. Sorlie, J. Stein, A. Towfighi, T. N. Turan, S. S. Virani, D. Woo, R. W. Yeh, and M. B. Turner, "Heart disease and stroke statistics–2016 update: A report from the American Heart Association," Circulation **133**(4), e38–e360 (2016).
2. A. Alonso and A. P. Arenas de Larriva, "Atrial fibrillation, cognitive decline and dementia," Eur Cardiol **11**(1), 49–53 (2016).
3. D. H. Tang, A. M. Gilligan, and K. Romero, "Economic burden and disparities in healthcare resource use among adult patients with cardiac arrhythmia," Appl. Health Econ. Health Policy **12**(1), 59–71 (2014).
4. J. G. Andrade, L. Rivard, and L. Macle, "The past, the present, and the future of cardiac arrhythmia ablation," Can. J. Cardiol. **30**(12), S431–S441 (2014).
5. K. Nishida, T. Datino, L. Macle, and S. Nattel, "Atrial fibrillation ablation: translating basic mechanistic insights to the patient," J. Am. Coll. Cardiol. **64**(8), 823–831 (2014).
6. M. Bohnen, W. G. Stevenson, U. B. Tedrow, G. F. Michaud, R. M. John, L. M. Epstein, C. M. Albert, and B. A. Koplan, "Incidence and predictors of major complications from contemporary catheter ablation to treat cardiac arrhythmias," Heart Rhythm **8**(11), 1661–1666 (2011).

#335515 https://doi.org/10.1364/BOE.9.006400
Journal © 2018 Received 25 Jun 2018; revised 4 Sep 2018; accepted 5 Sep 2018; published 20 Nov 2018

Biomedical Optics EXPRESS

7. M. D. Olson, N. Phreaner, J. L. Schuller, D. T. Nguyen, D. F. Katz, R. G. Aleong, W. S. Tzou, R. Sung, P. D. Varosy, and W. H. Sauer, "Effect of catheter movement and contact during application of radiofrequency energy on ablation lesion characteristics," J. Interv. Card. Electrophysiol. **38**(2), 123–129 (2013).
8. G. A. Pang, E. Bay, X. L. Deán-Ben, and D. Razansky, "Three-dimensional optoacoustic monitoring of lesion formation in real time during radiofrequency catheter ablation," J. Cardiovasc. Electrophysiol. **26**(3), 339–345 (2015).
9. D. Scherr, P. Khairy, S. Miyazaki, V. Aurillac-Lavignolle, P. Pascale, S. B. Wilton, K. Ramoul, Y. Komatsu, L. Roten, A. Jadidi, N. Linton, M. Pedersen, M. Daly, M. O'Neill, S. Knecht, R. Weerasooriya, T. Rostock, M. Manninger, H. Cochet, A. J. Shah, S. Yeim, A. Denis, N. Derval, M. Hocini, F. Sacher, M. Haissaguerre, and P. Jais, "Five-year outcome of catheter ablation of persistent atrial fibrillation using termination of atrial fibrillation as a procedural endpoint," Circ Arrhythm Electrophysiol **8**(1), 18–24 (2015).
10. R. Weerasooriya, P. Khairy, J. Litalien, L. Macle, M. Hocini, F. Sacher, N. Lellouche, S. Knecht, M. Wright, I. Nault, S. Miyazaki, C. Scavee, J. Clementy, M. Haissaguerre, and P. Jais, "Catheter ablation for atrial fibrillation: are results maintained at 5 years of follow-up?" J. Am. Coll. Cardiol. **57**(2), 160–166 (2011).
11. G. J. Wynn, M. El-Kadri, I. Haq, M. Das, S. Modi, R. Snowdon, M. Hall, J. E. Waktare, D. M. Todd, and D. Gupta, "Long-term outcomes after ablation of persistent atrial fibrillation: an observational study over 6 years," Open Heart **3**(2), e000394 (2016).
12. H. Calkins, K. H. Kuck, R. Cappato, J. Brugada, A. J. Camm, S. A. Chen, H. J. G. Crijns, R. J. Damiano, Jr., D. W. Davies, J. DiMarco, J. Edgerton, K. Ellenbogen, M. D. Ezekowitz, D. E. Haines, M. Haissaguerre, G. Hindricks, Y. Iesaka, W. Jackman, J. Jalife, P. Jais, J. Kalman, D. Keane, Y. H. Kim, P. Kirchhof, G. Klein, H. Kottkamp, K. Kumagai, B. D. Lindsay, M. Mansour, F. E. Marchlinski, P. M. McCarthy, J. L. Mont, F. Morady, K. Nademanee, H. Nakagawa, A. Natale, S. Nattel, D. L. Packer, C. Pappone, E. Prystowsky, A. Raviele, V. Reddy, J. N. Ruskin, R. J. Shemin, H. M. Tsao, and D. Wilber, "2012 HRS/EHRA/ECAS expert consensus statement on catheter and surgical ablation of atrial fibrillation: recommendations for patient selection, procedural techniques, patient management and follow-up, definitions, endpoints, and research trial design," Heart Rhythm **9**(4), 632–696 (2012).
13. V. Y. Reddy, D. Shah, J. Kautzner, B. Schmidt, N. Saoudi, C. Herrera, P. Jaïs, G. Hindricks, P. Peichl, A. Yulzari, H. Lambert, P. Neuzil, A. Natale, and K. H. Kuck, "The relationship between contact force and clinical outcome during radiofrequency catheter ablation of atrial fibrillation in the TOCCATA study," Heart Rhythm **9**(11), 1789–1795 (2012).
14. G. R. Vergara, S. Vijayakumar, E. G. Kholmovski, J. J. E. Blauer, M. A. Guttman, C. Gloschat, G. Payne, K. Vij, N. W. Akoum, M. Daccarett, C. J. McGann, R. S. Macleod, and N. F. Marrouche, "Real-time magnetic resonance imaging-guided radiofrequency atrial ablation and visualization of lesion formation at 3 Tesla," Heart Rhythm **8**(2), 295–303 (2011).
15. V. Ozenne, S. Toupin, P. Bour, A. Emilien, F. Vaillant, B. D. de Senneville, P. Jaïs, E. Dumont, J. Benois-Pineau, P. Desbarats, and B. Quesson, "Magnetic Resonance Imaging guided cardiac radiofrequency ablation," IRBM **36**(2), 86–91 (2015).
16. D. N. Stephens, J. Cannata, A. Nikoozadeh, O. Oralkan, A. de la Rama, A. Dentinger, D. Wildes, K. E. Thomenius, K. K. Shung, K. Shivkumar, A. Mahajan, M. O'Donnell, P. Khuri-Yakub, and D. J. Sahn, "Ultrasound compatible RF ablation electrode design for catheter based guidance of RF ablation - In vivo results with thermal strain imaging," 2010 IEEE Int. Ultrason. Symp. **2010**, 229–232 (2010).
17. D. N. Stephens, U. T. Truong, A. Nikoozadeh, O. Oralkan, C. H. Seo, J. Cannata, A. Dentinger, K. Thomenius, A. de la Rama, T. Nguyen, F. Lin, P. Khuri-Yakub, A. Mahajan, K. Shivkumar, M. O'Donnell, and D. J. Sahn, "First in vivo use of a capacitive micromachined ultrasound transducer array-based imaging and ablation catheter," J. Ultrasound Med. **31**(2), 247–256 (2012).
18. M. Wright, E. Harks, S. Deladi, F. Suijver, M. Barley, A. van Dusschoten, S. Fokkenrood, F. Zuo, F. Sacher, M. Hocini, M. Haïssaguerre, and P. Jaïs, "Real-time lesion assessment using a novel combined ultrasound and radiofrequency ablation catheter," Heart Rhythm **8**(2), 304–312 (2011).
19. M. Wright, E. Harks, S. Deladi, S. Fokkenrood, F. Zuo, A. Van Dusschoten, A. F. Kolen, H. Belt, F. Sacher, M. Hocini, M. Haïssaguerre, and P. Jaïs, "Visualizing intramyocardial steam formation with a radiofrequency ablation catheter incorporating near-field ultrasound," J. Cardiovasc. Electrophysiol. **24**(12), 1403–1409 (2013).
20. N. Dana, L. Di Biase, A. Natale, S. Emelianov, and R. Bouchard, "In vitro photoacoustic visualization of myocardial ablation lesions," Heart Rhythm **11**(1), 150–157 (2014).
21. C. P. Fleming, K. J. Quan, and A. M. Rollins, "Toward guidance of epicardial cardiac radiofrequency ablation therapy using optical coherence tomography," J. Biomed. Opt. **15**(4), 041510 (2010).
22. C. P. Fleming, H. Wang, K. J. Quan, and A. M. Rollins, "Real-time monitoring of cardiac radio-frequency ablation lesion formation using an optical coherence tomography forward-imaging catheter," J. Biomed. Opt. **15**(3), 030516 (2010).
23. C. P. Fleming, K. J. Quan, H. Wang, G. Amit, and A. M. Rollins, "In vitro characterization of cardiac radiofrequency ablation lesions using optical coherence tomography," Opt. Express **18**(3), 3079–3092 (2010).
24. C. P. Fleming, N. Rosenthal, and A. M. Rollins, "First in vivo real-time imaging of endocardial radiofrequency ablation by optical coherence tomography: implications on safety and the birth of "electro-structural" substrate-guided ablation," Innov. Card. Manag. **2**(3), 199–201 (2011).

Biomedical Optics EXPRESS

25. H. Wang, W. Kang, T. Carrigan, A. Bishop, N. Rosenthal, M. Arruda, and A. M. Rollins, "In vivo intracardiac optical coherence tomography imaging through percutaneous access: toward image-guided radio-frequency ablation," J. Biomed. Opt. **16**(11), 110505 (2011).
26. X. Fu, Z. Wang, H. Wang, Y. T. Wang, M. W. Jenkins, and A. M. Rollins, "Fiber-optic catheter-based polarization-sensitive OCT for radio-frequency ablation monitoring," Opt. Lett. **39**(17), 5066–5069 (2014).
27. D. Herranz, J. Lloret, S. Jiménez-Valero, J. L. Rubio-Guivernau, and E. Margallo-Balbás, "Novel catheter enabling simultaneous radiofrequency ablation and optical coherence reflectometry," Biomed. Opt. Express **6**(9), 3268–3275 (2015).
28. D. Herranz, S. Jiménez-Valero, C. L. Aramburu, J. Lloret, J. L. Rubio-Guivernau, and E. Margallo-Balbás, "Percutaneous RF ablation guided by polarization-sensitive optical coherence reflectometry in an integrated catheter: experimental evaluation of the procedure," JICRM **8**, 2086 (2015).
29. C. Hitzenberger, E. Goetzinger, M. Sticker, M. Pircher, and A. Fercher, "Measurement and imaging of birefringence and optic axis orientation by phase resolved polarization sensitive optical coherence tomography," Opt. Express **9**(13), 780–790 (2001).
30. B. Holmbom, U. Näslund, A. Eriksson, I. Virtanen, and L. E. Thornell, "Comparison of triphenyltetrazolium chloride (TTC) staining versus detection of fibronectin in experimental myocardial infarction," Histochemistry **99**(4), 265–275 (1993).
31. A. González-Suárez, D. Herranz, E. Berjano, J. L. Rubio-Guivernau, and E. Margallo-Balbás, "Relation between denaturation time measured by optical coherence reflectometry and thermal lesion depth during radiofrequency cardiac ablation: Feasibility numerical study," Lasers Surg. Med. **50**(3), 222–229 (2018).
32. V. Y. Reddy, D. Shah, J. Kautzner, B. Schmidt, N. Saoudi, C. Herrera, P. Jaïs, G. Hindricks, P. Peichl, A. Yulzari, H. Lambert, P. Neuzil, A. Natale, and K. H. Kuck, "The relationship between contact force and clinical outcome during radiofrequency catheter ablation of atrial fibrillation in the TOCCATA study," Heart Rhythm **9**(11), 1789–1795 (2012).
33. B. H. Park, C. Saxer, S. M. Srinivas, J. S. Nelson, and J. F. de Boer, "In vivo burn depth determination by high-speed fiber-based polarization sensitive optical coherence tomography," J. Biomed. Opt. **6**(4), 474–479 (2001).
34. W. Kang, H. Wang, Y. Pan, M. W. Jenkins, G. A. Isenberg, A. Chak, M. Atkinson, D. Agrawal, Z. Hu, and A. M. Rollins, "Endoscopically guided spectral-domain OCT with double-balloon catheters," Opt. Express **18**(16), 17364–17372 (2010).
35. R. P. Singh-Moon, C. C. Marboe, and C. P. Hendon, "Near-infrared spectroscopy integrated catheter for characterization of myocardial tissues: preliminary demonstrations to radiofrequency ablation therapy for atrial fibrillation," Biomed. Opt. Express **6**(7), 2494–2511 (2015).
36. R. P. Singh-Moon, X. Yao, C. C. Marboe, and C. P. Hendon, "Optical spectroscopy facilitated characterization of acute atrial lesions," in *Cancer Imaging and Therapy* (Optical Society of America, 2016), paper JTu3A–39.
37. P. Whittaker, S. Zheng, M. J. Patterson, R. A. Kloner, K. E. Daly, and R. A. Hartman, "Histologic signatures of thermal injury: Applications in transmyocardial laser revascularization and radiofrequency ablation," Lasers Surg. Med. **27**(4), 305–318 (2000).

1. Introduction

In the past two decades, cardiac arrhythmias have become one of the direst public health issues and a major cause of health care expenditure in western countries [1]. They affect millions of people in the United States and are a significant cause of morbidity and mortality, leading to more than 400,000 sudden cardiac deaths annually [1]. Additionally, cardiac arrhythmias are a major risk factor for stroke and heart failure and have even been linked to the development of Alzheimer's disease [2]. Arrhythmias are also a major economic burden, costing the US healthcare system more than $67 billion annually [3]. Since its initial description in 1982, catheter-based radiofrequency ablation (RFA) through percutaneous access has been commonly practiced in interventional electrophysiology (EP) to treat cardiac arrhythmias. During the RFA procedure, a small catheter is guided into the heart to heat and destroy the culprit tissue that was causing abnormal electrical conduction with radiofrequency energy. This has become the standard of care for cardiac arrhythmias as it is often curative, eliminating the need for medications that potentially last a lifetime [4, 5]. Complication rates from the procedure are also low, with 0.8%-6% of patients experiencing a major complication depending primarily on the type of ablation and the patient's severity of illness [6].

Despite the success of RFA in treating many cardiac arrhythmias, challenges still remain. Currently, RFA lesion formation is monitored through indirect methods, such as temperature, impedance, electrograms, and contact force. Fluoroscopy and 3D catheter tracking provide gross guidance. This creates several challenges, including verifying catheter-tissue contact [7], monitoring and confirming lesion completion [8], detecting complication precursors, and

Biomedical Optics EXPRESS

visualizing tissue structures to target and avoid. These challenges result in long procedure times (2 to 8 hours depending on the type of the arrhythmia), higher recurrence rate, and compromised patient safety. Atrial fibrillation (AF), which is the most prevalent sustained arrhythmia in the western world, is especially difficult to treat, with a single procedure success rate as low as 17% after 5 years. Even with multiple procedures, 2.1 on average, the success rate is approximately 65% after 5 years [9–11]. One important reason for the high recurrence is insufficient direct, real-time guidance of the ablation which leads to incomplete (i.e., non-transmural) lesions or gaps in continuous lines of lesions [9, 12]. Direct feedback may also enable detection of complication precursors, identification of tissue structures, and confirmation of the quality of catheter-tissue apposition, which would result in faster, more accurate, and safer procedures.

To address some of these issues, multiple solutions have been proposed. Recently, force sensitive catheters have been rapidly adopted by EP practitioners to confirm catheter-tissue contact force and angle. Since poor contact force and improper contact angles have been shown to directly correlate with increased recurrence due to poor lesion quality, these catheters give the provider feedback on lesion quality in real time [13]. Unfortunately, this information is only an estimate extrapolated from research data and not a direct measurement of the quality of an individual lesion. Therefore, it does not completely meet the clinical need. Magnetic resonance imaging (MRI) has been used to monitor the formation of RFA lesions [14, 15]. However, the low resolution and expensive specialized equipment limits the use of MRI-based RFA procedures. An ultrasound integrated RFA electrode probe for RFA procedure guidance has been reported [16, 17], but the image resolution and contrast is low. An M-scan ultrasound integrated RFA catheter has been proposed to assess the lesion formation and prevent complications from steam pops in real time [18, 19]. However, it cannot provide catheter-tissue contact and tissue substrate information, which is very important for procedure guidance. Others have reported direct monitoring of RFA lesion formation with photoacoustic technology [8, 20], but these systems have not been tested *in vivo* and currently suffer from a very low frame rate and low imaging resolution. Additionally, the diameter of the photoacoustic probe is greater than 10 mm, which limits its usage, especially in pediatric arrhythmia treatment. Near-infrared spectroscopy (NIRS) has also been reported to monitor lesion formation by sensing tissue endogenous metmyoglobin content changes caused by ablation [35, 36], but it has not been shown to provide enough information to identify tissue structure.

Previously, we proposed that an RFA catheter with integrated optical coherence tomography (OCT) imaging can address many of the current challenges with RFA. OCT imaging provides real-time, in-depth imaging of biological tissues with high spatial resolution (on the order of ten micrometers). We have previously demonstrated (both *in vitro* [21–23, 26] and *in vivo* [24, 25]) that direct imaging feedback from catheter-based OCT can confirm catheter contact and angle [24, 25], identify tissue structures [21,25], confirm ablation lesion formation [21–24, 26], and may detect precursors of complication, like gas formation ahead of steam pops [22, 24, 25]. We have also shown that the loss of birefringence in cardiac tissue, which can be easily detected by PSOCT, is a strong marker of thermal ablation and has the potential to provide feedback during lesion formation [22, 26, 27]. Herranz *et al.* have described an RFA catheter integrated with optical coherence reflectometry (M-mode OCT, not imaging) to monitor the RF ablation process in *real time* based on the loss of birefringence [27, 28, 31]. However, like NIRS, it has not been shown to identify tissue substrates.

Taken together, these encouraging previous studies have demonstrated that integrating PSOCT imaging into the RFA catheter may be able to address all of the unmet clinical needs outlined above, and therefore has the potential to reduce procedure time, recurrence, and improve safety.

Biomedical Optics EXPRESS

However, these previous studies have used either bench-top OCT systems, stand-alone OCT probes, or non-imaging probes. To further validate the clinical potential of this technology, an integrated RFA/OCT catheter is needed that is capable of delivering radiofrequency energy and acquiring PSOCT images simultaneously. In this paper, we demonstrate an integrated 2.3mm (7 Fr) diameter RFA/OCT catheter for monitoring RFA procedures with PSOCT imaging in real time. The integrated RFA/OCT catheter was modified from a standard clinical RFA catheter to include a miniature forward-viewing cone-scanning OCT probe. Key imaging and ablation functions are demonstrated experimentally.

2. Methods

2.1 Integrated catheter design

To test the feasibility of an integrated RFA/OCT catheter, a standard clinical 2.3mm (7 Fr) RFA catheter (Blazer II HTD, Boston Scientific) was modified to incorporate an OCT probe while maintaining the RFA functionality. Figure 1(a) illustrates the design of the integrated RFA/PSOCT catheter. The steering cable and thermocouple inside the RFA catheter were removed to provide space for the OCT components, while maintaining the basic RFA functionality. After removing the thermocouple, a resistor was used to keep the catheter registerable with the RF generator, but this disabled the temperature sensing functionality of the catheter. A 1.0 mm diameter hole was made in the distal tip of the electrode to accommodate imaging. A glass window sealed the hole to isolate the OCT probe from the environment. Sealing was made with UV glue rated for temperatures above those generated in RFA. A simple, miniature, flexible, forward-viewing, cone-scanning OCT probe was inserted into the RFA catheter.

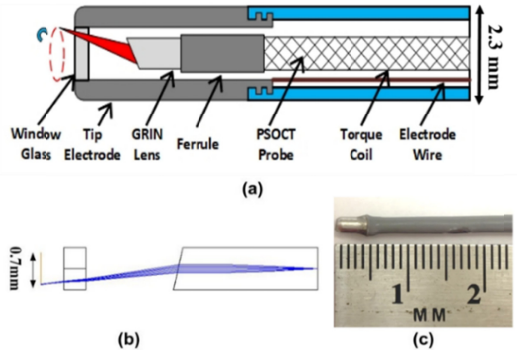

Fig. 1. (a) Schematic of the integrated RFA/OCT probe; (b) Zemax design of the OCT probe; (c) Photograph of the integrated RFA/OCT probe.

Figure 1(b) illustrates the Zemax design of the OCT probe, which is similar to our previous design [25]. Light from the optical fiber is focused by a 1.0 mm diameter gradient-index (GRIN) lens, and the end of the GRIN lens is polished at a 15-degree angle to deflect light from the center axis of the probe. The measured focused beam size is 15 μm at full-width at half maximum (FWHM). The GRIN lens was mounted to a 1.0 mm outer diameter flexible torque cable. As the output light is offset from the probe's center axis, a cone pattern is scanned by rotating the torque cable with a motor and fiber-optic rotary joint. The circumference of the scanned cone is about 2.0 mm at the focal point. Figure 1(c) shows a photograph of an integrated RFA/OCT catheter.

2.2 PSOCT system

To acquire the PSOCT images during the RFA procedure, the integrated RFA/OCT probe was connected to a PSOCT system and an RFA generator (see below). Figure 2 shows the schematic of the PSOCT system. A 50 kHz swept laser (AXP50125-6, Axsun Technologies,

Biomedical Optics EXPRESS

USA) with 20 mW average output power was used as the light source. A fiber Bragg grating (FBG) was used to generate a stable line trigger signal for data collection synchronization. Two fiber-based polarizing beam splitters (FPBS) and 2 balanced detectors (Det 1, 2) are used to collect the image data from two polarization channels. The intensity and retardance images are calculated from the 2 images obtained from these two channels with orthogonal polarizations [29]. To validate the retardance measurement accuracy, a zero-order quarter-wave plate was imaged in various fast-axis orientations, both with a fixed beam (M-mode) and rotating wave plate, and with a scanning beam and a fixed wave plate. In addition, a high-birefringence plastic phantom was imaged to validate the retardance contrast of the system.

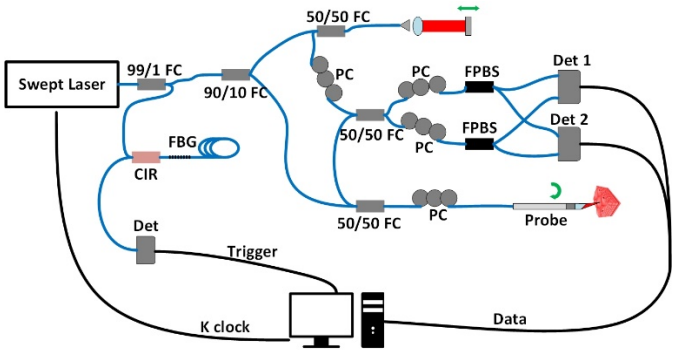

Fig. 2. Schematic of the PSOCT system for the integrated RFA/OCT probe. A 50 kHz Axsun swept source laser is used as the source. A fiber Bragg grating (FBG) is used to generate a stable trigger signal for the A-line collection. FC, fiber coupler; Det, detector (Det 1and 2 are balanced detectors); CIR, fiber circulator; PC polarization controller; FPBS, fiber based polarization beam splitter.

2.3 Sample preparation and experimental validation

Freshly excised swine hearts and freshly drained heparinized swine blood (from intra-vascular OCT catheter training swine, approved by the Institutional Animal Care and Use Committee of Case Western Reserve University) were used to test the RFA/OCT system. To keep the tissue fresh, it was kept in ice-cold phosphate-buffered saline (PBS) before imaging. The right ventricular (RV) free wall was carefully dissected for the study.

In order to test the impact of the glass window in the RFA electrode on lesion creation, two groups of RFA lesions were created in fresh RV samples using the integrated RFA/PSOCT catheter and an intact, unmodified commercial RFA catheter of the same model, respectively. A Maestro 3000 RFA generator (Boston Scientific) was used to generate two groups of lesions under the same ablation parameter setting (temperature control mode: 70°C, maximum delivery power: 50W, and ablation time: 20 seconds). As mentioned in 2.1, the thermocouple was removed during integration to make room for the OCT probe. For this experiment, to enable both catheters to operate in temperature control mode (more commonly used in clinical procedures compared to power control mode) for optimal comparison of lesion formation, the thermocouple of the integrated catheter was soldered to the external surface of the distal tip electrode to provide temperature sensing capabilities. (The thermocouple was not used for subsequent experiments described below.) Staining with 2,3,5-triphenyl-tetrazolium chloride (TTC) was used to validate lesion formation and quantify lesion size [23, 30]. TTC is a vital stain which has been widely used to differentiate necrotic from viable tissue in the acute setting [18]. By TTC staining, healthy tissue will present dark red color, while ablated tissue will be white. To compare the two groups of lesions, the lesions were imaged with a 10X microscope with a calibration marker to measure the size of the lesions at the tissue surface. Then, the lesions were sliced perpendicular to the tissue

Biomedical Optics EXPRESS

surface across the center of each lesion. Tissue samples were incubated in 1.0% TTC in phosphate buffered saline (PBS) for 30 minutes at 37°C. The TTC stained samples were then imaged by the same microscope to measure the lesion depth.

To test the functionality of the integrated catheter for evaluating tissue contact, fresh RV tissue was submerged in blood and imaged at various angles of contact. Finally, to test RFA lesion monitoring functionality, the dissected RV free wall was submerged in room temperature (20°C) PBS solution. A series of ablative lesions were created using the RF generator in power-control mode with a power limit of 20 W and duration of 50 sec. PSOCT images were recorded throughout both of these experiments.

3. Results

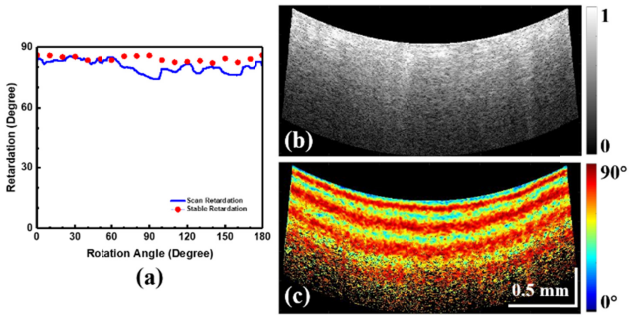

Fig. 3. (a) Measured phase retardation of a quarter-wave plate at different optical axis orientations (red dot); measured phase retardation of a quarter-wave plate with scanning catheter (blue line) using the PSOCT system; (b) Polarization insensitive intensity image of a high-birefringence plastic phantom using the PSOCT system; (c) Phase retardance image of the same phantom

To validate the integrated RFA/OCT system, both the PSOCT and the RFA energy delivery functions were tested independently. First, PSOCT imaging was verified. Results of the quarter-wave plate validation are shown in Fig. 3(a). The mean measured retardance was 85 degrees with a fixed beam and rotating sample, and 80.4 degrees for a rotating beam and fixed sample, which is acceptable for this application compared to the theoretical value of 90 degrees. As expected, there was more variation in the phase retardance measurement due to the change of incident polarization state caused by catheter rotation, compared to the fixed beam. This impact could be mitigated by referring to the incident polarization state at the sample surface. The system was then used to image a high-birefringence plastic phantom. For the cone-scanning images generated by the integrated catheter, the transverse scanning range increases with depth. Therefore, displaying the data as a conventional rectangular-shaped OCT image will distort the image. A fan-shaped display can maintain a uniform aspect ratio throughout the image [25], by "unwrapping" the 3-D cone into a 2-D fan. Figure 3(b) shows the fan-shaped polarization insensitive intensity image (calculated using both polarization channels) and Fig. 3(c) shows the fan-shaped phase retardance image of the plastic phantom. Due to the accumulative nature of the PSOCT retardance measurement, the high birefringence can clearly be seen as a dense banded structure. The retardance measurement is clear and stable as the OCT probe rotates. The results of Fig. 3 show that the PSOCT system can provide accurate phase retardance images as well as conventional OCT images.

To verify the RF energy delivery of the integrated catheter, 10 lesions were created with the integrated catheter and compared to 10 lesions created with an unmodified standard clinical RFA catheter of the same model. The same RFA generator and ablation protocol were used for both catheters. The results are shown in Table 1 and Fig. 4. The lesion width and depth shown in Table 1 are similar between the two catheters, indicating that the glass window had no significant impact on RF energy delivery.

Biomedical Optics EXPRESS

Table 1. Size of Lesions from Control and Integrated Catheters (Mean ± SD)

Catheter	Lesion Number	Width(mm)	Depth(mm)
Standard Commercial Probe	10	3.5 ± 0.4	1.8 ± 0.2
Integrated RFA/OCT Probe	10	3.6 ± 0.4	1.7 ± 0.1

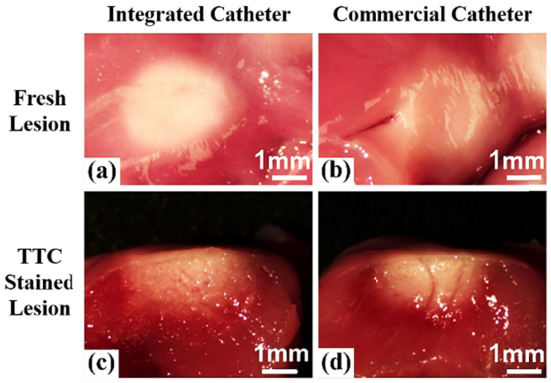

Fig. 4. Images of representative RFA lesions. (a, b) Tissue surface images of fresh lesions from the integrated RFA/OCT probe and unmodified commercial catheter, respectively, (c, d) Images of TTC stained cross-sections of lesions in (a, b), respectively.

The system monitored catheter-tissue apposition in real time. To assess catheter-tissue contact, OCT images were recorded in real time while the integrated catheter was manipulated in various positions relative to blood-immersed tissue. Illustrations of the orientation as well as representative, corresponding images are shown in Fig. 5. Figures 5(a) and (e) show the catheter when it is not in contact with the tissue. In Fig. 5(e), only blood can be seen in the image. Due to high signal attenuation by blood, the penetration is very shallow. While the catheter approaches the tissue surface, the layer of blood becomes thinner and the tissue surface can be seen as shown in Fig. 5(b) and (f). Since the layer of blood is not uniform, the image indicates that the catheter is approaching the tissue at an angle. The tissue structure is poorly visualized due to the light attenuation by the blood. Figures 5(c) and (g) show the case when the catheter is making contact with the tissue at an angle. Blood on the right side of the image results in decreased tissue penetration, similar to Fig. 5(f). While tissue structure is well visualized on the left side of the image, which indicates partial tissue contact. Figures 5(d) and (h) show a diagram and image when the catheter is contacting the tissue perpendicularly. The tissue structure can be seen in the whole field of view, which indicates the catheter is in perpendicular contact with tissue. These distinct features in the OCT images correspond well with different catheter-tissue appositions, demonstrating that integrated OCT imaging can guide catheter-tissue contact. This experiment was repeated three times with equivalent results.

Biomedical Optics EXPRESS

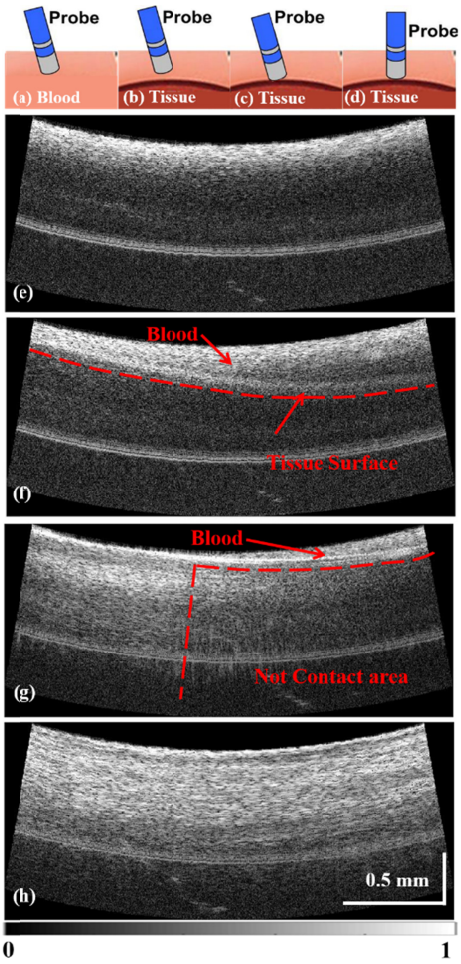

Fig. 5. Assessment of catheter-tissue contact with OCT images. (a), (e): The catheter position and OCT image when the catheter is not in contact with the tissue. (b), (f): The catheter position and OCT image when the catheter is approaching the tissue. (c), (g): The catheter position and OCT image when the catheter is making partial contact with the tissue (tilted contact). (d), (h): The catheter position and OCT image when the catheter is in full contact with the tissue (perpendicular contact).

PSOCT monitoring of RFA lesion formation was also tested. In this experiment, the integrated catheter was used to acquire PSOCT images in real time during delivery of RF energy. Figure 6 shows real-time PSOCT intensity images and retardance images acquired at 0, 15, 27, and 45 seconds from the start of RFA energy delivery for a representative lesion. In Fig. 6(a)-(d), the OCT intensity images can be seen. These show that the tissue becomes more scattering as the lesion forms. The PSOCT images can be seen in Fig. 6(e)-(h), which demonstrate that the birefringence signal (false colored) gradually disappears as the lesion forms. This provides a much stronger indication of tissue treatment than the OCT intensity images alone. This experiment was repeated nine times. In all cases, similar changes in the intensity images and the distinct disappearance of retardance were observed. The ablation time to reach disappearance of retardance varied from 33 to 43 sec. This time variability likely resulted from natural variability in the RV tissue substrate.

Biomedical Optics EXPRESS

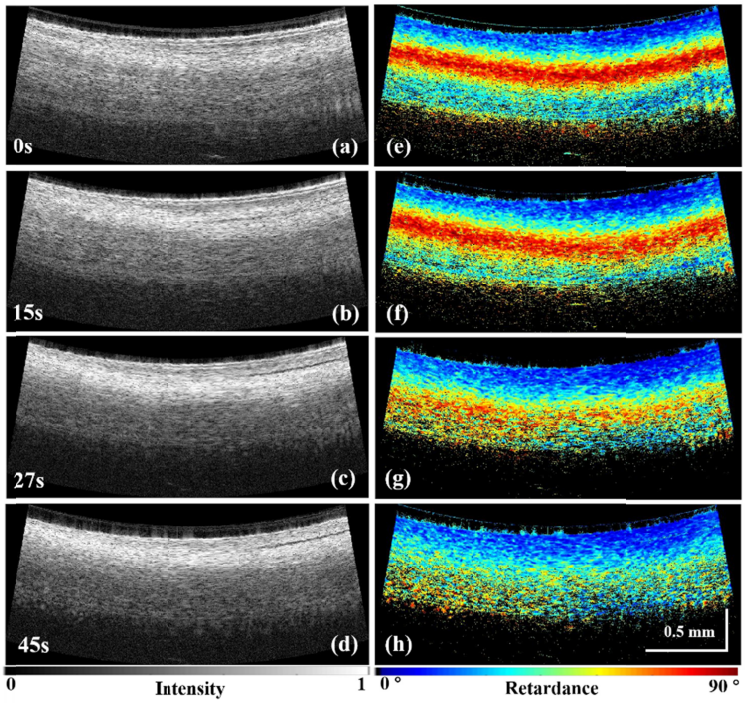

Fig. 6. Real-time monitoring of RFA lesion formation with the integrated RFA/OCT catheter. (a)-(d) OCT images of the tissue during the application of RFA energy at 0, 15, 27 and 45 seconds. (e)-(h) Phase retardance images of the tissue at the corresponding times. From (e)-(h), with the application of the RF energy, the birefringence of the tissue becomes weaker and weaker, and disappears after 45 seconds.

4. Discussion

RF ablation has been broadly adopted as a first line treatment for many arrhythmias (e.g. atrial flutter, atrial ventricular reentrant tachycardia, atrial ventricular nodal reentrant tachycardia) and is becoming the first line treatment for others, including atrial fibrillation. Because of this, better procedural guidance is needed to increase the acute success rate, reduce the recurrence rate, reduce procedure time, and improve safety. Here, we demonstrate a high resolution imaging technique with polarization contrast that can be used to guide catheter tissue contact and directly monitor lesion formation in real time. For this proof-of-principle experiment, RV tissue was used as sample due to the relatively uniform thickness and tissue structure.

The integrated catheter prototype used for these experiments was made by modifying a commercial RF catheter. This included modification of the catheter tip to integrate a glass window, which results in a smaller RF electrode surface area. This could potentially cause changes in energy delivery. To determine whether lesions would form properly, lesions formed by the integrated catheter and unmodified commercial catheter were compared. The results shown in Table 1 and Fig. 4 demonstrate that the lesions created by the two different catheters are similar in width and depth. This indicates that the modifications made to the commercial RFA catheter had no significant effect on RFA energy delivery and lesion formation. One potential source of error in these measurements is that contact force was not measured or controlled. However, the same apparatus was used to maintain catheter-tissue contact, and the same experimental procedure was used with both catheters, so we do not believe that contact force was systematically different between the two catheters. It is possible that the different position of the thermal sensor in the integrated catheter could have led to

Biomedical Optics EXPRESS

biased results, but no evidence from the experiment indicated that this was the case. Future prototype catheters will incorporate temperature sensing in the electrode (which will obviate this concern) and will be tested using this same approach.

A potential benefit of this technology is direct feedback of catheter-tissue contact and apposition. This contact information would be useful for EP practitioners because it impacts lesion formation and allows EP practitioners to produce high quality lesions in multiple different scenarios. For example, when creating a point lesion, the optimum orientation is for the catheter to be perpendicular to the tissue; when dragging the catheter to create a line lesion, the catheter needs to be oriented at an angle and maintain contact. Having direct feedback of the catheter-tissue contact and angle allows the EP practitioners to verify apposition in real time. As demonstrated above in Fig. 5, non-contact, tilted contact, and complete perpendicular contact can be readily differentiated by observing the features of the blood and tissue in the acquired OCT images. Additionally, the images allow EP practitioners to understand the approach angle before the tissue is even contacted. The recent, rapid adoption of force-sensing catheters is evidence of the significant value of real-time catheter-tip apposition feedback. In addition to quality and angle of contact, contact force has been shown to impact lesion quality, size, and rate of arrhythmia recurrence and is an important piece of information for physicians [32]. Images may provide valuable complementary information to force feedback. In addition, we have previously shown that endoscopic OCT images of gastrointestinal mucosa clearly depict tissue structural deformation in response to catheter pressure [34]. In the future, we will investigate the relationship between observed tissue deformation and lesion quality, and the potential of predicting and confirming lesion quality directly from OCT images.

To validate the lesion monitoring functionality of the integrated catheter, PSOCT images were obtained throughout the ablation process. As noted above, Fig. 6 shows that during ablation, the tissue becomes more reflective in the OCT intensity images, while the birefringence signal disappears in the PSOCT images, providing much stronger contrast. The disappearance of the birefringence signal indicates that the proteins composing the oriented fiber structure have been thermally denatured by the RF energy [33]. This result is consistent with our previous report and has also been reported in the literature as a reliable marker for irreversible muscle injury in the myocardium [22, 37]. Due to the depth limitation of PSOCT imaging, the denaturing process can only be monitored to around 1 mm in depth. However, the depth of an optimal lesion in the ventricle is usually deeper than 2 mm, so the full extent of the lesion will not always be directly visible with PSOCT imaging. Therefore, more experiments are warranted to correlate loss of birefringence (including the dynamics of the process) with lesion depth, and to investigate monitoring of lesion placement in the atrium, which has thinner walls but more complicated tissue structures. Though additional investigation is required, the current results indicate that the RFA/OCT integrated catheter can be used to confirm and monitor lesion formation, and that the retardance signal from PSOCT provides clear, strong contrast during lesion formation.

5. Conclusion

In conclusion, we prototyped and demonstrated a 2.3 mm (7 Fr) diameter, flexible, integrated, RFA/OCT catheter, which can be used to monitor RFA lesion formation with PSOCT imaging in real time. The integration of the OCT probe into a commercial RFA catheter did not affect lesion formation. With this integrated catheter, catheter-tissue contact was readily characterized by observing the features of the blood and tissue in the acquired OCT images. RFA lesions can also be confirmed by the loss of birefringence in the heart tissue.

Direct imaging by OCT has the potential to improve guidance during RFA procedures ensuring catheter-tissue contact and providing real-time monitoring and confirmation of lesion formation. Importantly, this may decrease procedure time and fluoroscopy imaging time, therefore reduce radiation exposure to the patient and physician. Furthermore, real-time

Biomedical Optics EXPRESS

feedback from OCT during RFA therapy may potentially decrease recurrence rates and procedural complications by allowing real-time confirmation of lesion quality and detecting potential complications early. In the future, the objective is to improve the integrated catheter for real-time monitoring of the RFA procedure *in vivo*.

Funding

National Institutes of Health (NIH) (R21CA165398, R21HL129174, R01HL083048); Case-Coulter Translational Research Partnership; China Scholarship Council.

Acknowledgments

The authors would like to thank Dr. Steve Schomisch for his help with swine hearts procurement.

Disclosures

The authors declare that there are no conflicts of interest related to this article.